

# Genuine multipartite entanglement as a probe of many-body localization in disordered spin chains with Dzyaloshinskii–Moriya interactions

Triyas Sapui<sup>1</sup>, Keshav Das Agarwal<sup>1</sup>, Tanoy Kanti Konar<sup>1</sup>, Leela Ganesh Chandra Lakkaraju<sup>1,2,3</sup>, Aditi Sen (De)<sup>1</sup>

<sup>1</sup> *Harish-Chandra Research Institute, A CI of Homi Bhabha National Institute, Chhatnag Road, Jhansi, Allahabad - 211019, India*

<sup>2</sup> *Pitaevskii BEC Center and Department of Physics, University of Trento, Via Sommarive 14, I-38123 Trento, Italy and*

<sup>3</sup> *INFN-TIFPA, Trento Institute for Fundamental Physics and Applications, Trento, Italy*

We demonstrate that the quenched average genuine multipartite entanglement (GME) can approach its maximum value in the ergodic phase of a disordered quantum spin model. In contrast, GME vanishes in the many-body localized (MBL) phase, both in equilibrium and in the long-time dynamical steady state, indicating a lack of useful entanglement in the localized regime. To establish this, we analyze the disordered Heisenberg spin chain subjected to a random magnetic field and incorporating two- and three-body Dzyaloshinskii–Moriya (DM) interactions. We exhibit that the behavior of GME, in both static eigenstates and in dynamically evolved states from an initial Néel configuration, serves as a reliable indicator of the critical disorder strength required for ergodic to MBL transition. The identified transition point aligns well with standard indicators such as the gap ratio and correlation length. Moreover, we find that the presence of DM interactions, particularly the three-body one, significantly stabilizes the thermal phase and delays the onset of localization. This shift in the transition point is consistently reflected in both static and dynamical analyses, reinforcing GME as a robust probe for MBL transitions.

## I. INTRODUCTION

Quantum statistical mechanics posits that isolated, interacting many-body systems generically thermalize under unitary evolution, meaning local observables reach thermal equilibrium values described by the Gibbs ensemble, effectively erasing memory of initial conditions. This behavior is encapsulated in the eigenstate thermalization hypothesis (ETH) [1–3], which asserts that individual energy eigenstates exhibit thermal properties, rendering the system ergodic. ETH explains how unitary evolution aligns with statistical mechanics, as eigenstates in the bulk of the spectrum become locally indistinguishable and featureless. These systems exhibit quantum chaos and ergodicity [4], reflected in their energy level statistics [5–7] described by the Wigner-Dyson distribution [8, 9] in Gaussian random matrix ensembles such as Gaussian orthogonal ensembles (GOE) for real matrices or Gaussian unitary ensembles (GUE) for complex matrices. However, ETH can be violated in systems exhibiting integrability [10], many-body scars [11, 12], Stark localization [13], Floquet dynamics [14, 15], or non-Hermitian effects [16, 17], leading to non-ergodic behavior and preventing thermalization.

ETH breaking was first explored through disorder-induced localization in non-interacting systems, known as Anderson localization [18]. In recent decades, its many-body counterpart, many-body localization (MBL), emerged in interacting disordered systems [19, 20]. Extensive research has been devoted to this exotic phenomenon across various systems, including spinless fermions [19, 21], spin chains [20, 22] and Hubbard model [23–25] along with long-range interactions [26–31], highlighting the apparent universality [32, 33] and emergent integrability in MBL, characterized by an extensive set of local integrals of motion (l-bits) [34–36]. Despite these efforts and several experimental works [37–44], a comprehensive understanding of the transition between the ergodic and MBL phases remains elusive, with several theoretical models proposed [45–50]. Key signatures of the MBL phase include Poisson level statistics [7, 51], correlation pat-

terns [52, 53], and quantum order [54–59]. Such systems also possess unique dynamical traits, depicted by the absence of transport [60], long-time memory of the initial state(s) characterized by imbalance [61–64], dynamical ergotropy [65], slow growth of entanglement entropy [66–68] and magic [69] following a disordered quench.

The block entanglement entropy, which changes from a volume law in the ergodic phase to an area law in the MBL phase [54, 70–74] as well as bipartite entanglement [75, 76] turn out to be key indicators for determining the ergodic-to-MBL transition. Dynamically, disorder-induced slow growth of entanglement also marks the MBL transition [66–68]. However, studies of multipartite entanglement, a natural faithful quantity for understanding phenomena in many-body systems, remain limited (see recent works considering multisite physical quantities like quantum Fisher information [77–80], entanglement spectra [81, 82], Schmidt gaps [83] and quantum mutual information [84, 85] although they cannot quantify multipartite quantum correlations properly).

In this work, we address this gap by utilizing a computable measure of genuine multipartite entanglement for pure states, namely generalized geometric measure (GGM) [86–91], defined via the minimum distance from non-genuinely multipartite entangled states [92], to analyze a class of disordered many-body Hamiltonians. Specifically, we investigate a spin-1/2 Heisenberg chain with a randomly chosen magnetic field in the presence of multi-body Dzyaloshinskii–Moriya (DM) interaction [93–95]. Originating from spin-orbit coupling, the DM interaction introduces an antisymmetric exchange term between spins and has been widely studied in systems such as the nearest-neighbor and long-range transverse Ising [96–98], XY [99–101], and the gamma models [102], where it can induce gapless chiral phases and enhance  $zz$ -correlations when its strength surpasses anisotropy. Further, it has been found in various solid-state systems, including  $\text{Cu}(\text{C}_6\text{D}_5\text{COO})_2 \cdot 3\text{D}_2\text{O}$ ,  $\text{Yb}_4\text{As}_3$  to name a few [103–107]. Moreover, the DM interaction plays a compelling role in the context of many-body localization, as it breaks time-

reversal symmetry and changes the spectral statistics from GOE to GUE while preserving the system's  $\mathbb{U}(1)$  symmetry.

We explore the influence of both two- and three-body DM interactions both in the ergodic and MBL regimes. Our analysis reveals that three-body DM interactions have a more significant impact in delaying the ergodic-to-MBL transition than the two-body DM term (cf. [108]), thereby extending the thermal phase. We analyze the eigenstates of the disordered Hamiltonian and find that the profile of quenched average genuine multipartite entanglement, measured by GGM [92], successfully tracks the ergodic to MBL transition, which is in good agreement with conventional measures such as spectral statistics and long-range correlator. In particular, the quenched average GGM values and the maximum of probability distribution for GGM are high in the ergodic phase but drop significantly in the MBL phase.

By initializing the system in a Néel state and evolving it under the similar class of Hamiltonians, we demonstrate that the trends of multipartite entanglement during both transient and steady-state regimes reveal a delayed ergodic-to-MBL transition in the presence of DM interactions, marked by distinct changes in the proposed scaling laws. These observations align well with known indicators such as imbalance [62–64]. Notably, high multipartite entanglement is generated in both short and long time periods of the ergodic phase, whereas the MBL phase exhibits significantly reduced entanglement. This comprehensive study highlights the impact of DM interactions on localization phenomena and firmly establishes multipartite entanglement as a reliable indicator for disorder-induced phase transitions.

The paper is organized as follows. In Sec. II, we describe the model and the relevant quantifiers such as GGM in Sec. II A 1, level statistics in Sec. II B 1, and long-range classical correlators in Sec. II B 2. We then use the GGM to characterize the MBL to ergodic transition and compare it with the traditional measures in Sec. III which is further divided into the study of Heisenberg model without and with DM interaction in Secs. III A and III B respectively. We also perform finite size scaling in the Sec. IV. Dynamics of GGM is studied in Sec. V and we finally conclude in Sec. VI.

## II. INTRODUCING MODEL AND TRANSITION INDICATORS

We consider a spin-1/2 one-dimensional Heisenberg model subject to a random external magnetic field along the  $z$ -direction, introducing disorder into the system. It also includes both two-body and three-body Dzyaloshinskii–Moriya interactions [93–95]. The Hamiltonian of the system reads as

$$H = J \sum_{k=1}^N \vec{S}_k \cdot \vec{S}_{k+1} + \tilde{D} (S_k^x S_{k+1}^y - S_k^y S_{k+1}^x) + 2\tilde{D}' (S_k^x S_{k+1}^z S_{k+2}^y - S_k^y S_{k+1}^z S_{k+2}^x) + \tilde{h}_k S_k^z, \quad (1)$$

where  $S_k^a = \sigma_k^a/2$  ( $a = \{x, y, z\}$ ) are the spin operators and  $\sigma_k^a$  are the Pauli matrices at site  $k$  with periodic boundary condition ( $S_{k+N}^a \equiv S_k^a$ ). To eliminate energy dependence

in all figures of merit, we redefine the random magnetic field as  $h_k = \tilde{h}_k/J$ , sampled uniformly from the interval  $[-h, h]$  and  $D = \tilde{D}/J$  and  $D' = \tilde{D}'/J$ , denoting the strengths of the two-body and three-body DM interactions, respectively. The  $\mathbb{U}(1)$  symmetry present in the disordered Heisenberg chain is preserved by the inclusion of both two- and three-body DM interactions, as they conserve the total magnetization,  $S^z = \sum_{k=1}^N S_k^z$ , i.e.,  $[H, S^z] = 0$  even when  $D, D' \neq 0$ . This allows the Hamiltonian to be block-diagonalized into magnetization sectors labeled by  $S^z \in \{-N/2, -N/2+1, \dots, N/2\}$ . In our analysis, we restrict ourselves to the  $S^z = 0$  sector (and even  $N$ ), which has the largest Hilbert space among all  $S^z$  blocks. Without the DM interaction, the model is well-studied and is known to undergo a transition from ergodic to MBL phase [20]. In this work, we focus on the effects of two- and three-body interaction on the transition and utilize an information-theoretic quantity for its detection, which also provides information about the model's suitability in quantum information protocols.

*Set the stage to identify transition point.* To characterize the phases in this model, we choose a physical quantity of interest and perform quenched averaging over different disorder realizations. In particular, the given quantity is computed by averaging over both the eigenstates and the disorder realizations. We consider the  $n_\varepsilon$  number of eigenstates from the middle spectrum of the Hamiltonian to compute the expectation value of a physical quantity, denoted as  $\langle O \rangle = \frac{1}{n_\varepsilon} \sum_{j=1}^{n_\varepsilon} \langle \psi_j | O | \psi_j \rangle$  where  $|\psi_j\rangle$  are the  $n_\varepsilon$  eigenstates with eigenvalue close to 0, i.e., the middle of the spectrum. Subsequently, an averaging over  $n_R$  randomly chosen disorder realizations is carried out to compute the quenched average quantity as  $\overline{\langle O \rangle}$ . Eigenstates are obtained via exact diagonalization [109] till  $N = 14$ , and through POLFED [110] for system sizes  $N = 16$  and 18 (see Appendix A). We select the corresponding values of  $n_\varepsilon$  and  $n_R$  by performing a convergence check up to the desired accuracy for a given system size  $N$  (see Table I), by computing the standard deviation of averaged values of  $n_R/10$  realizations. In case of dynamics, an average over  $n'_R$  realizations is taken to compute quenched average dynamical quantity,  $\overline{O(t)}$  at each time  $t$  (see Table I). The behavior of  $\overline{O(t)}$  is used to distinguish between the ergodic and the MBL phases.

### A. Multipartite entanglement quantifier to disclose transition

Let us first introduce the information-theoretic measure, in particular, genuine multipartite entanglement measure, based on geometry of the state space [111].

#### 1. Quantifier for genuine multiparty entanglement

A pure  $N$ -party state  $|\Psi_{1,2,\dots,N}\rangle$ , is genuinely multiparty entangled (GME) if it is not product across any bipartition. Based on Fubini-Study metric, a quantification of GME content of a state is possible, known as generalized geometric measure (GGM) [89, 92, 111, 112]. It is defined as the min-

| $N$ | $n_\epsilon$    | $n_R$           | $n'_R$          |
|-----|-----------------|-----------------|-----------------|
| 8   | 22              | $10^4$          | $5 \times 10^3$ |
| 10  | 80              | $10^4$          | $3 \times 10^3$ |
| 12  | $2 \times 10^2$ | $5 \times 10^3$ | $2 \times 10^2$ |
| 14  | $4 \times 10^2$ | $2 \times 10^3$ | $10^3$          |
| 16  | $8 \times 10^2$ | $5 \times 10^2$ | $10^3$          |
| 18  | $10^3$          | $10^2$          | -               |

TABLE I. The table indicates the number of eigenstates  $n_\epsilon$  picked from the middle of the spectrum and  $n_R$  is the number of realizations taken for performing quenched averaging for a given system-size  $N$ .  $n'_R$  is the number of realizations taken in the case of dynamics with disorder system.

imum distance from the set of all non-genuinely (nG) multipartite entangled states, i.e.,

$$\mathcal{G}(|\Psi\rangle) = 1 - \max_{|\chi\rangle} |\langle \chi | \Psi \rangle|^2, \quad (2)$$

where  $|\chi\rangle$  belongs to the set of nG entangled states. An equivalent expression for the above can be given as

$$\mathcal{G}(|\Psi\rangle) = 1 - \max_{A:B} [\lambda_{A:B}^2 |A \cap B = \emptyset, |A \cup B| = N], \quad (3)$$

in which the maximization is carried out over all bipartitions  $A : B$ , and  $\lambda_{A:B}$  denotes the largest eigenvalues in the corresponding bipartition. Although it is computable measure for moderate  $N$  in arbitrary dimension, the computation of  $\mathcal{G}(|\Psi\rangle)$  becomes numerically intensive due to exponential increase of the number of such bipartitions with the system-size  $N$ . Hence, this computational complexity necessitates the use of approximations in calculating the GGM.

To mitigate this challenge, we simplify our approach by restricting attention to Schmidt coefficients obtained from all single-site reduced density matrices. With this simplification, we define the geometric measure (GM), also a multipartite entanglement measure, as

$$\mathcal{G}_1(|\Psi\rangle) = 1 - \max_{A:B, |A|_{\max}=1} [\lambda_{A:B}^2 |A \cap B = \emptyset, |A \cup B| = N], \quad (4)$$

where the maximization is performed only over bipartitions for which  $A$  consists of a single spin. To validate the effectiveness of this approximation in the problem addressed here, we compute both  $\mathcal{G}$  and  $\mathcal{G}_1$  for all eigenstates of various system-sizes. We find that  $|\langle \mathcal{G} - \mathcal{G}_1 \rangle| \approx e^{-N}$  (see Fig. 1) which decreases rapidly with increasing system size, indicating that the  $\mathcal{G}_1$  is as effective as  $\mathcal{G}$  in characterizing multipartite entanglement. Therefore, in the rest of this paper, we use  $\mathcal{G}$  and  $\mathcal{G}_1$  alternatively as there is no such distinction between these two quantity to quantify phases which can help in studying the role of two- and three-body DM interaction in altering the phases in Heisenberg spin chain, which we study in the next section. Note that the computational resource for calculating

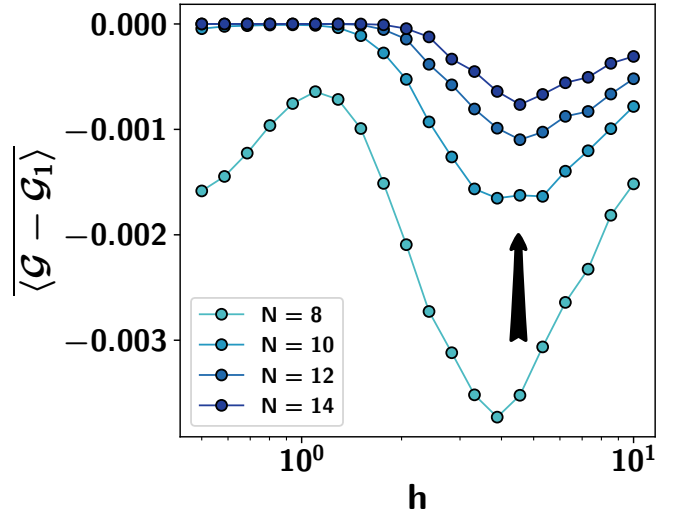


FIG. 1. The difference between the exact GGM,  $\mathcal{G}$ , and its single-site approximation,  $\mathcal{G}_1$ , i.e.,  $\langle \mathcal{G} - \mathcal{G}_1 \rangle$  (ordinate) against the disorder strength,  $h$  for increasing system sizes. It reveals that as the system-size grows, the difference vanishes. This trend suggests that  $\langle \mathcal{G}_1 \rangle$  serves as an accurate alternative for the genuine multipartite entanglement and can be used in place of  $\langle \mathcal{G} \rangle$  in these systems. All axes are dimensionless.

GGM ( $\mathcal{G}_1$ ) of a generic eigenstate of a many-body Hamiltonian does not grow significantly with system size as it depends only on the single-site density matrices of the eigenstate.

*Estimating maximum eigenvalues via randomized measurements.* We note that the estimation of extremal spectral properties, particularly the largest eigenvalue of a quantum state required to compute GGM, can be efficiently approximated through the recently developed randomized measurement toolbox [113]. This framework allows for the construction of a so-called classical shadow  $\hat{\rho}$  of the true quantum state  $\rho$  by performing randomized local unitary and projective measurements on a computational basis. Crucially, the quality of this estimate can be quantified using the operator norm, i.e., by computing a deviation between the actual and estimated states as the probability that the estimated classical shadow  $\hat{\rho}$  is  $\epsilon$ -close to  $\rho$  is given by  $\mathbb{P}(\|\hat{\rho} - \rho\|_\infty < \epsilon) < 1 - \kappa$ , where  $\kappa$  is a logarithmic function of the number of measurements and the dimension of the state  $\rho$ .

Invoking Weyl's inequality [114], which bounds the deviation in eigenvalues by the operator norm difference, the estimated maximum eigenvalue  $\lambda_{\max}^{\text{est}}$  and the true maximum eigenvalue  $\lambda_{\max}^{\text{og}}$  obey the inequality  $|\lambda_{\max}^{\text{og}} - \lambda_{\max}^{\text{est}}| < \|\hat{\rho} - \rho\|_\infty$ . We may use this to obtain

$$\mathbb{P}(|\lambda_{\max}^{\text{og}} - \lambda_{\max}^{\text{est}}| < \epsilon) < 1 - \kappa, \quad (5)$$

thereby asserting that the classical shadow framework can provide a faithful estimation of the maximum eigenvalues without requiring full quantum state tomography. This renders the approach particularly suitable for scalable entanglement diagnostics in many-body systems, where exact state reconstruction can be expensive.

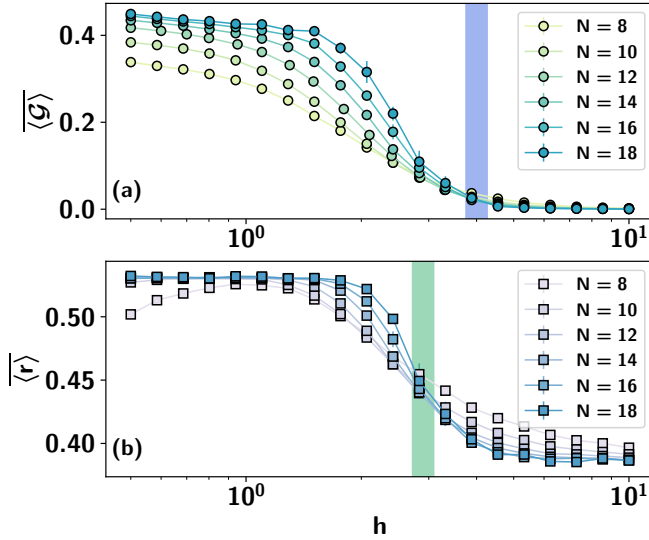


FIG. 2. The quenched averaged GGM, denoted by  $\overline{\langle \mathcal{G} \rangle}$  (ordinate), and the average gap ratio,  $\overline{\langle r \rangle}$  (ordinate), are displayed as functions of the disorder strength  $h$  (abscissa) in the upper (a) and lower (b) panels of the figure, respectively. Both quantities are plotted for increasing system sizes  $N$ , illustrating that  $\overline{\langle \mathcal{G} \rangle}$  serves as an equally effective indicator as  $\overline{\langle r \rangle}$  in identifying the ergodic to many-body localized phase transition in the Heisenberg model ( $D = D' = 0$ ). The critical disorder strength is estimated to be  $h^* = 4.0$  for GGM, while for the gap ratio,  $h^* = 2.9$ . All axes are dimensionless.

### B. Conventional transition detectors

We now briefly discuss two physical quantities that are commonly used to probe the ergodic-to-MBL transition.

#### 1. Level statistics for benchmarking

A method, referred to as level statistics, has been extensively utilized in the literature to identify MBL phase due to its distinct behavior in the ergodic and MBL phases of the disordered model. Since its inception, it has been established that the energy level spacings of a non-integrable Hamiltonian typically follow a Wigner-Dyson distribution [8, 9], while those of an integrable Hamiltonian adhere to a Poisson distribution [7, 51]. One commonly used quantity to characterize level statistics is the gap ratio, defined as

$$r_n = \frac{\min(\Delta_n, \Delta_{n-1})}{\max(\Delta_n, \Delta_{n-1})}, \quad (6)$$

where  $\Delta_n = E_{n+1} - E_n$  represents the spacing between two consecutive energy levels,  $n+1$  and  $n$  with  $\{E_j\}$  representing the eigenenergies of the Hamiltonian. A quenched average gap ratio,  $\overline{\langle r \rangle} = 0.5307$  indicates that the system is ergodic and falls within the Gaussian orthogonal ensemble (GOE), corresponding to the Wigner-Dyson distribution. Conversely, if  $\overline{\langle r \rangle} = 0.3863$ , the level statistics are Poissonian, signifying

that the system resides in an MBL phase. Moreover, for systems that break time-reversal symmetry, the spectral statistics follow the GUE, characterized by  $\overline{\langle r \rangle} = 0.5996$ .

#### 2. Long-range classical correlators

Another useful transition indicator is the average long-range classical correlator, defined as

$$C_r^{zz} \equiv C_{ij}^{zz} = \langle \psi | S_i^z S_j^z | \psi \rangle - \langle \psi | S_i^z | \psi \rangle \langle \psi | S_j^z | \psi \rangle, \quad (7)$$

where  $|i - j| = r$  and  $|\psi\rangle$  is a state from the middle of the energy spectrum of the Hamiltonian. Pal and Huse argued that in the ergodic phase,  $\langle \psi | S_j^z | \psi \rangle \sim 0$  due to the system being in the  $S^z = 0$  sector, although a finite long-range correlation due to the first term persists between distant spins [20]. In contrast, in the MBL phase,  $\langle \psi | S_j^z | \psi \rangle$  acquires a finite value and the long-range correlation decays exponentially with increasing spin separation.

It will be interesting to examine how  $\overline{\langle \mathcal{G} \rangle}$  detects the transition point in the presence of two- and three-body DM interactions in comparison with  $\overline{\langle r \rangle}$  and  $\langle \ln |C_r^{zz}| \rangle$ .

## III. CHARACTERIZING PHASES WITH DZYALOSHINSKII-MORIYA INTERACTION

To establish the GGM as a faithful quantity to indicate the ergodic to MBL transition, we first perform the study over the well-studied Heisenberg model, i.e., when  $D = D' = 0$  in Eq. (1) and then carry out the investigation for  $D \neq 0$  as well as  $D' \neq 0$ . We then report the performance of GGM to differentiate the phases in the presence of two- and three-body DM interactions. In addition, we propose the distribution of the GGM over the eigenstates of the Hamiltonian as a novel indicator that can differentiate two phases.

### A. MBL and ergodic phases in Heisenberg model

A clear one-to-one correspondence between  $\overline{\langle \mathcal{G} \rangle}$  and  $\overline{\langle r \rangle}$ , indicates that multisite entanglement effectively captures the MBL transition (see Fig. 2(a) for  $\overline{\langle \mathcal{G} \rangle}$  and Fig. 2(b) for  $\overline{\langle r \rangle}$ ). Specifically, for the Heisenberg spin chain model ( $D = D' = 0$ ), the transition is observed near  $\sim 3.3$  through the measure  $\overline{\langle \mathcal{G} \rangle}$ , which is in a good agreement with previous results [20], mentioning the MBL transition at  $h^* = 3.5$ . This transition point can be consistently verified by the standard indicator  $\overline{\langle r \rangle}$ , which takes the value  $\overline{\langle r \rangle} \sim 0.53$  in the ergodic phase ( $h < h^*$ ) while it drops to  $\overline{\langle r \rangle} \sim 0.39$  in the MBL phase ( $h > h^*$ ). On the other hand, in the ergodic regime ( $h < h^*$ ),  $\overline{\langle \mathcal{G} \rangle}$  saturates to a finite value, approximately  $\overline{\langle \mathcal{G} \rangle} \sim 0.5$ , with this feature becoming more pronounced as the system-size increases. In contrast,  $\overline{\langle \mathcal{G} \rangle}$  slowly decreases and eventually vanishes with the increase of the disorder strength beyond the transition point  $h^*$ . The pattern of  $\overline{\langle \mathcal{G} \rangle}$  with  $h$  also reveals



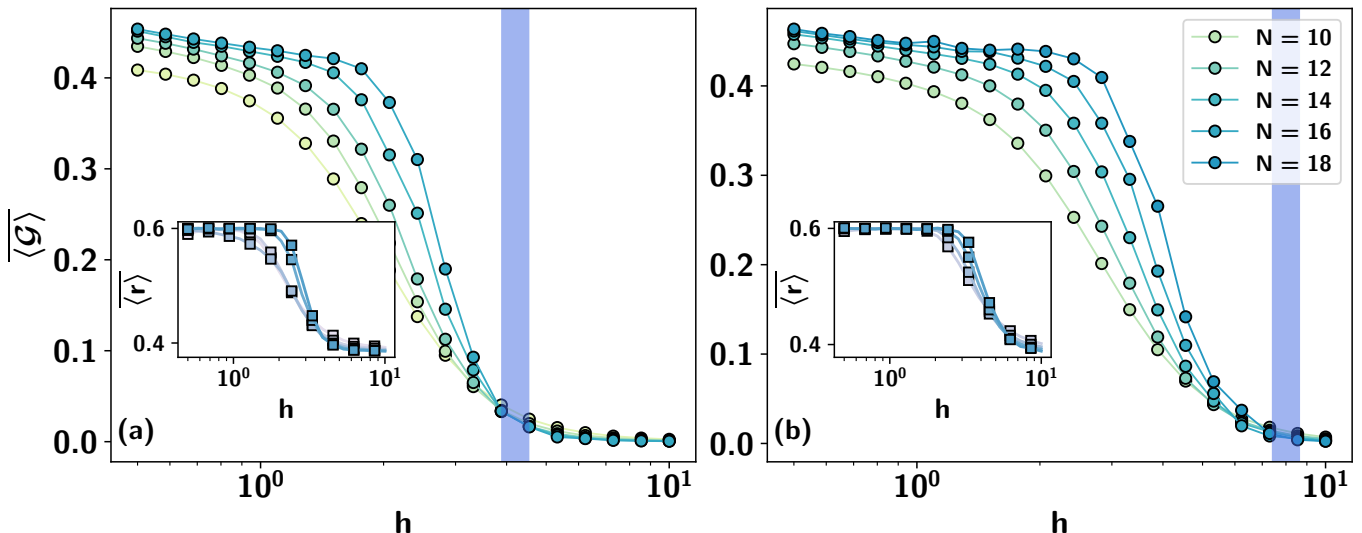


FIG. 3.  $\overline{\langle \mathcal{G} \rangle}$  (ordinate) against disorder strength  $h$  (abscissa) for increasing system sizes, considering both (a) two-body and (b) three-body Dzyaloshinskii–Moriya (DM) interactions. These plots exhibit a transition from the ergodic phase to the many-body localized one, similar to the transition identified using the gap ratio  $\overline{\langle r \rangle}$  (shown in the insets of both figures). The critical disorder strength is estimated to be  $h^* = 3.9$  for the two-body DM interaction and  $h^* = 7.9$  for the three-body DM interaction, indicated by a solid vertical bar. It is evident that DM interaction can extend the ergodic phase and delay the transition. All axes are dimensionless.

another interesting point – the multisite entanglement is high at the ergodic phase, it decreases with moderate  $h$  value and finally vanishes at the MBL phase. This result suggests that MBL phase may be unsuitable for building quantum devices that rely on multipartite entanglement to function effectively.

Let us provide an intuitive explanation for why GGM effectively captures the MBL transition, as well as the saturation of  $\overline{\langle \mathcal{G} \rangle}$  to characteristic values in both the ergodic and MBL regimes. This behavior of  $\overline{\langle \mathcal{G} \rangle}$  can be understood through the lens of random matrix theory (RMT). In the ergodic phase, the system’s Hamiltonian is expected to follow RMT predictions, where the eigenstates resemble Haar-random pure states. From the perspective of entanglement theory, Haar-random multipartite states are known to exhibit high multipartite entanglement on average with the increase of number of sites [115–117]. Consequently, the eigenstates in the thermal (ergodic) regime display a high average GGM, close to the value  $\sim 0.5$ . On the other hand, as the disorder strength increases and the system enters the MBL phase, multipartite entanglement gets strongly suppressed, leading to the vanishing GGM. These findings reinforce the validity of  $\overline{\langle \mathcal{G} \rangle}$  as a robust and insightful marker of the MBL transition, and the above argument suggests its potential universality across disordered systems.

### B. Extended ergodic phase in Heisenberg model with DM interaction detectable via GGM

The nearest-neighbor DM interaction arises due to spin-orbit coupling, induces long-range correlation among distant spins and manifests as an antisymmetric exchange interaction

between spins [93–95]. Such interactions have recently become experimentally accessible in quantum simulators [118]. We explore here the consequence (impact) of the DM interaction in modulating the transition from the ergodic to the many-body localized phase in the Heisenberg chain.

*Influence of two-body DM interactions on transition.* The inclusion of a two-body DM interaction alters the behavior of both  $\overline{\langle \mathcal{G} \rangle}$  and the gap ratio. Importantly, since the DM interaction breaks time-reversal symmetry, as mentioned before, the spectral statistics exhibit behavior consistent with GUE class, instead of GOE. Hence, in the ergodic regime,  $\overline{\langle r \rangle}$  approaches 0.6 as the system-size  $N$  increases, which is characteristic of the GUE statistics, as shown in the inset of Fig. 3(a) by the solid lines. The level statistics exhibit a transition from the ergodic to the MBL phase as the disorder strength increases, with  $\overline{\langle r \rangle}$  decreasing from 0.6 to 0.39. However, in the presence of DM interaction, the ergodic phase is extended, requiring a higher disorder strength to induce the transition to the MBL phase. Interestingly, the trends of  $\overline{\langle \mathcal{G} \rangle}$  also signal a delayed ergodic-to-MBL transition, as stronger disorder is needed for the GGM to completely vanish in the MBL phase. Specifically, we observe that for  $D = 0.5$  ( $D' = 0$ ),  $h^* \sim 3.9$  (see Fig. 3(a)). Note that the location of the transition is dictated by the strength of the DM interaction, which implies more deferment of the transition with a higher  $D$  values. This observation suggests that the ergodic phase becomes more robust under the influence of DM interaction. In this regime, the enhanced correlations introduced by the DM term necessitate a stronger disorder to localize the system and induce the MBL phase.

*Three-body DM interaction delays the transition significantly.* Instead of two-body DM interaction, let us incorpo-

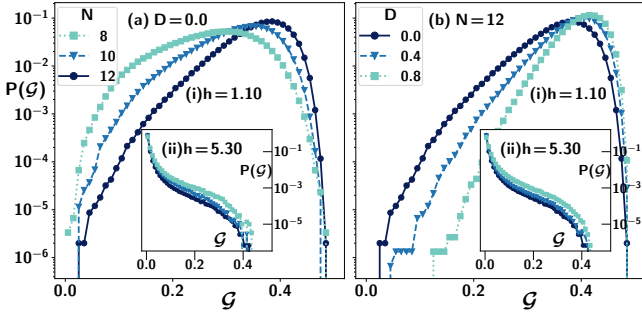


FIG. 4. Distribution of GGM  $\mathcal{G}(|\psi_i\rangle)$ ,  $P(\mathcal{G})$  (ordinate) vs  $\mathcal{G}$  for eigenvectors  $|\psi_i\rangle$  in the middle spectrum of various realizations in distribution of magnetic field  $h_k \in [-h, h]$  at each site  $k$ . (a) For  $D = 0$ , the GGM of states tends to  $\mathcal{G} \sim 0.4$  for large number of states with increase in system-size  $N$  in the thermalized regime (shown for  $h = 1.1$ ). (Inset of (a)) In the localized region for  $h = 5.3$ , larger number of states has GGM  $\mathcal{G} \sim 0.01$  on increasing system-size  $N$ . (b) With varying DM interactions, the ensemble has a higher GGM which increases with increasing two-body DM interactions  $D$ , both in the thermalized and localized (inset of (b)) region. All the axes are dimensionless.

rate three-body DM interactions, i.e.,  $D = 0, D' \neq 0$  in Eq. (1). Again, the DM interaction is responsible for further postponement of the transition point, i.e.,  $h^*$ . In particular, the transition to the MBL phase is further delayed compared to the two-body interaction, with a critical disorder strength of approximately  $h^* = 7.9$ , (see Fig. 3(b)) obtained via  $\langle \mathcal{G} \rangle$  which is also in a good agreement with  $h^*$ , predicted by  $\langle r \rangle$ . These values are calculated via analysis of finite-size scaling in Sec. IV. This prolonged thermal phase can be attributed to the next-nearest-neighbor (NNN) hopping induced by the three-body DM interaction. Such hopping enhances delocalization, thereby promoting ergodicity. However, strong local perturbations, such as a disordered external magnetic field, suppress this hopping mechanism, thereby facilitating localization and leading to the MBL phase at sufficiently high disorder strength. The next step is to investigate the distribution of GGM across the full spectrum of eigenstates, and how this distribution evolves with the introduction of the DM interaction.

*Distribution of GGM as a transition marker.* An important question that arises is how multipartite correlations, such as  $\mathcal{G}$  of the eigenstates, are distributed across the ergodic and MBL phases. We demonstrate that in the ergodic phase, the distribution of  $\mathcal{G}$  is sharply peaked near its maximum value, indicating that most eigenstates exhibit nearly maximal multipartite entanglement. The frequency distribution of  $\mathcal{G}$  is defined as  $P(\mathcal{G}) = \frac{|\mathcal{S}_\epsilon(\mathcal{G})|}{n_{RN_\epsilon}}$  where  $|\mathcal{S}_\epsilon(\mathcal{G})| = |\{|\psi_j\rangle, \mathcal{G}(|\psi_j\rangle) \in [\mathcal{G} - \epsilon, \mathcal{G} + \epsilon]\}|$  is the cardinality of the set of eigenstates with the GGM value  $\mathcal{G}(|\psi_j\rangle)$   $\epsilon$ -close to  $\mathcal{G}$  ( $\epsilon = 5 \times 10^{-3}$  for Fig. 4). The observations in the absence of DM interactions can be listed as follows: (1a) In the absence of DM interaction,  $P(\mathcal{G})$  corresponding to the highest  $\mathcal{G}$  value dominates, while the distribution exhibits an exponential decay as  $\mathcal{G}$  deviates from its maximum. (1b) System-size also plays a significant role – as

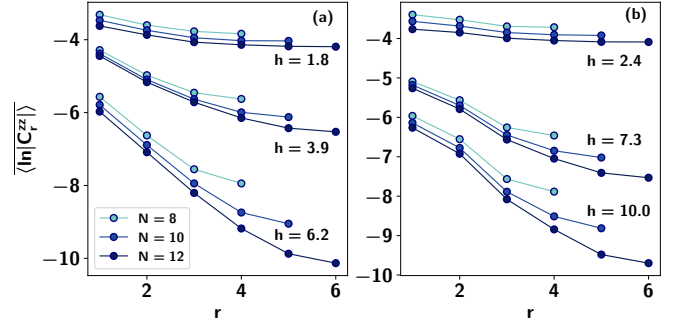


FIG. 5.  $\langle \ln |C_r^{zz}| \rangle$  (ordinate) against the distance between the spins,  $r$  (abscissa). We plot the decay of long-range correlation in the  $z$ -direction with  $r$  for different disorder strengths with two- and three-body DM interactions for different systems-sizes. (a) For two-body DM interaction ( $D = 0.5, D' = 0$ ), in the ergodic phase  $\langle \ln |C_r^{zz}| \rangle$  saturates to a fixed value, which is very high, denoting the presence of strong correlation due the DM term. On the other hand, in the MBL phase, such correlation decays exponentially as seen for  $h = 6.2$ . (b) Introduction of three-body DM interaction – a similar trait is observed for  $D = 0$ , and  $D' = 0.5$ , higher disorder strength of  $h$  is required to transit from ergodic to MBL phases. For instance, corresponding to  $h = 6.2$  in (a), similar behavior emerges when  $h = 10$ . All the axes are dimensionless.

the system-size increases, the peak of the  $\mathcal{G}$ -distribution converges towards a saturated value of approximately  $\sim 0.5$ . (1c) In the MBL phase, the peak of the distribution shifts toward lower values of  $\mathcal{G}$ , closer to zero, indicating that eigenstates in the MBL regime possess significantly lower multipartite entanglement (see the inset of Fig. 4(a)). (2a) When two- and three-body DM interactions are introduced, the ergodic phase is extended, and the peak of the  $\mathcal{G}$ -distribution quickly shifts towards its maximum value as the strength of the DM interaction increases (see Fig. 4(b)). In other words, with the increase of  $D$ , the standard deviation of  $P(\mathcal{G})$  decreases. (2b) Additionally, the frequency of states with maximum  $\mathcal{G}$  increases with the DM interaction strength, suggesting that the DM interaction enhances long-range correlations among spins. Consequently, the number of highly entangled eigenstates grows with increasing DM interaction strength.

*Increment of long-range correlation in presence of DM interaction.* Let us now argue that the delay in the ergodic to MBL transition in the presence of DM interaction can be due to persistent LR correlations,  $\langle \ln |C_r^{zz}| \rangle$ , in the systems. For all values of  $h$ , it decays with distance  $r$ , although the decay rate varies with the disorder strength. In particular, when  $D = D' = 0$ , the decay of  $\langle \ln |C_r^{zz}| \rangle$  is slower for  $h$  belonging to the deep ergodic phase while its decay is rapid in the MBL phase [20]. In the presence of DM interaction, we find that even for moderate to large  $h$  values, the decay rate is small and it gets larger only when the disorder strength is strong enough (see Figs. 5 (a) and (b)). Further, the LR correlation value itself of the Heisenberg model with non-vanishing DM interaction becomes higher compared to the case without DM interactions. For example, at a fixed system-size  $N = 12$  and distance  $r = 6$ ,  $\langle \ln |C_r^{zz}| \rangle \sim -10.5$  for  $h = 6.23$  and

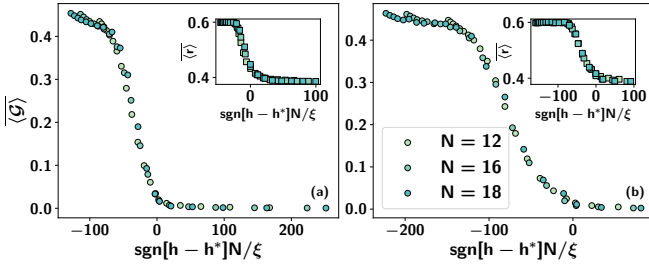


FIG. 6. Finite-size scaling analysis of the averaged GGM and level spacing (in insets) in presence of two- (a) and three-body (b) DM interactions. For three different system sizes,  $N = 12, 16$  and  $18$ ,  $\overline{\langle G \rangle}$  (ordinate) against  $\text{sgn}[h - h^*]N/\xi$  (abscissa). Interestingly, we obtain the scaling exponent and critical disorder strength which is independent of system-size. The resulting values and the exponents obtained are reported in Table II. All the axis are dimensionless.

$\langle \ln |C^{zz}| \rangle \sim -4.5$  for  $h = 1.77$  for  $D = 0.5, D' = 0$  (see Fig. 5(a)), while similar  $\langle \ln |C^{zz}| \rangle$  values ( $\sim -10.5$  and  $\sim -4.5$ ) are obtained for higher  $h$  ( $h = 10.0$  and  $h = 2.41$  respectively), when  $D = 0, D' = 0.5$  (see Fig. 5(b)). As a result, stronger disorder strength is needed to observe the onset of exponential decay, indicating a delayed transition to the MBL phase. In both the two-body and three-body DM interaction scenarios, the long-range correlation decays exponentially at sufficiently large disorder strength, which is a hallmark of the MBL phase. These findings confirm that the DM interaction enhances the correlations between spins and effectively extends the ergodic phase which is also responsible for high multipartite entanglement in the system.

#### IV. FINITE-SIZE SCALING ANALYSIS FOR TRANSITION

The divergence of the correlation length is a central concept in the theory of critical phenomena and phase transitions. The transition from the ergodic to the many-body localized phase is typically characterized by a power-law divergence of the correlation length of classical correlators. In such scenarios, the correlation length diverges as

$$\xi = \frac{1}{|h - h^*|^\nu}, \quad (8)$$

where  $\nu$  is the critical exponent.  $h^*$  denotes the critical disorder strength. In this study, we fix the value of  $h^*$  and perform a finite-size scaling analysis to obtain scale-invariant observables  $\tilde{X} \equiv X(N/\xi)$ . This can be accomplished by minimizing a cost function  $C^X$  [22, 32, 33, 72, 119], to quantify the quality of data collapse. The cost function is given by

$$C^X = \frac{\sum_{k=1}^{N_{\text{tot}}-1} |X_{k+1} - X_k|}{\max\{X_k\} - \min\{X_k\}} - 1, \quad (9)$$

where  $N_{\text{tot}}$  are the number of data points corresponding to different values of disorder strength  $h$ , system size  $N$ , and

all  $X_k$  values are sorted in non-decreasing order according to the rescaled variable  $\text{sgn}[h - h^*]N/\xi$ . An ideal data collapse yields a cost function  $C^X = 0$ . We perform finite-size scaling analysis for both the average gap ratio  $r$  and the multipartite entanglement measure  $\overline{\langle G \rangle}$ , for the random Heisenberg model as well as for cases involving two- and three-body DM interactions.

| Interaction Type  | Quantity                       | $h^*$ | $\nu$ |
|-------------------|--------------------------------|-------|-------|
| $D = 0, D' = 0$   | $\overline{\langle r \rangle}$ | 2.9   | 0.8   |
|                   | $\overline{\langle G \rangle}$ | 4.0   | 1.4   |
| $D = 0.5, D' = 0$ | $\overline{\langle r \rangle}$ | 3.4   | 0.7   |
|                   | $\overline{\langle G \rangle}$ | 3.9   | 1.1   |
| $D = 0, D' = 0.5$ | $\overline{\langle r \rangle}$ | 6.3   | 1.2   |
|                   | $\overline{\langle G \rangle}$ | 7.9   | 1.7   |

TABLE II. Critical disorder strength  $h^*$  and critical exponent  $\nu$  from scaling analysis of  $\overline{\langle r \rangle}$  and  $\overline{\langle G \rangle}$  for different interaction types.  $h^*$  obtained from GGM is in a good agreement with the ones from the gap ratio. This also establishes the usefulness of GGM for the detection of ergodic to MBL phases.

In order to find out system size independent criticality in transition from ergodic to MBL phase, we perform finite size scaling in Fig. 6. The strength of the critical disorder,  $h^*$  and the scaling exponent,  $\nu$  changes with the introduction of DM interaction of two and three bodies, more precisely  $h^*$  increases with reference to the Heisenberg model, verified by both the quantifier,  $\overline{\langle r \rangle}$  and  $\overline{\langle G \rangle}$  as shown in Table II. On the other hand,  $h^*$  is higher in the case of a three-body DM interaction than the two-body DM interaction, indicating an increase of the ergodic region in the presence of a three-body DM interaction, as shown in Table II.

#### V. CAPTURING ERGODIC TO MBL TRANSITION VIA DYNAMICAL QUANTITY

The entire analysis performed in the previous sections is based on the properties of the eigenstates and eigenspectrum of the Hamiltonian. The multisite entanglement turns out to be a beneficial quantity for determining the transition from ergodic to MBL phase, apart from revealing the potentiality in quantum information tasks in the latter phase. Let us now assess whether the nature of multipartite entanglement with time can also carry signatures of the phases.

To answer this, let us consider the evolution of an initially unentangled state under a Hamiltonian residing either in the localized or in the ergodic phase. In the MBL phase, the system typically preserves substantial memory of the initial configuration owing to the inhibited transport of energy and other local observables. However, what distinguishes the MBL phase from its non-interacting counterpart, namely the Anderson localized phase, is the nontrivial manner in which quantum information, for example, entanglement, disperses across the system. A hallmark signature of this phenomenon

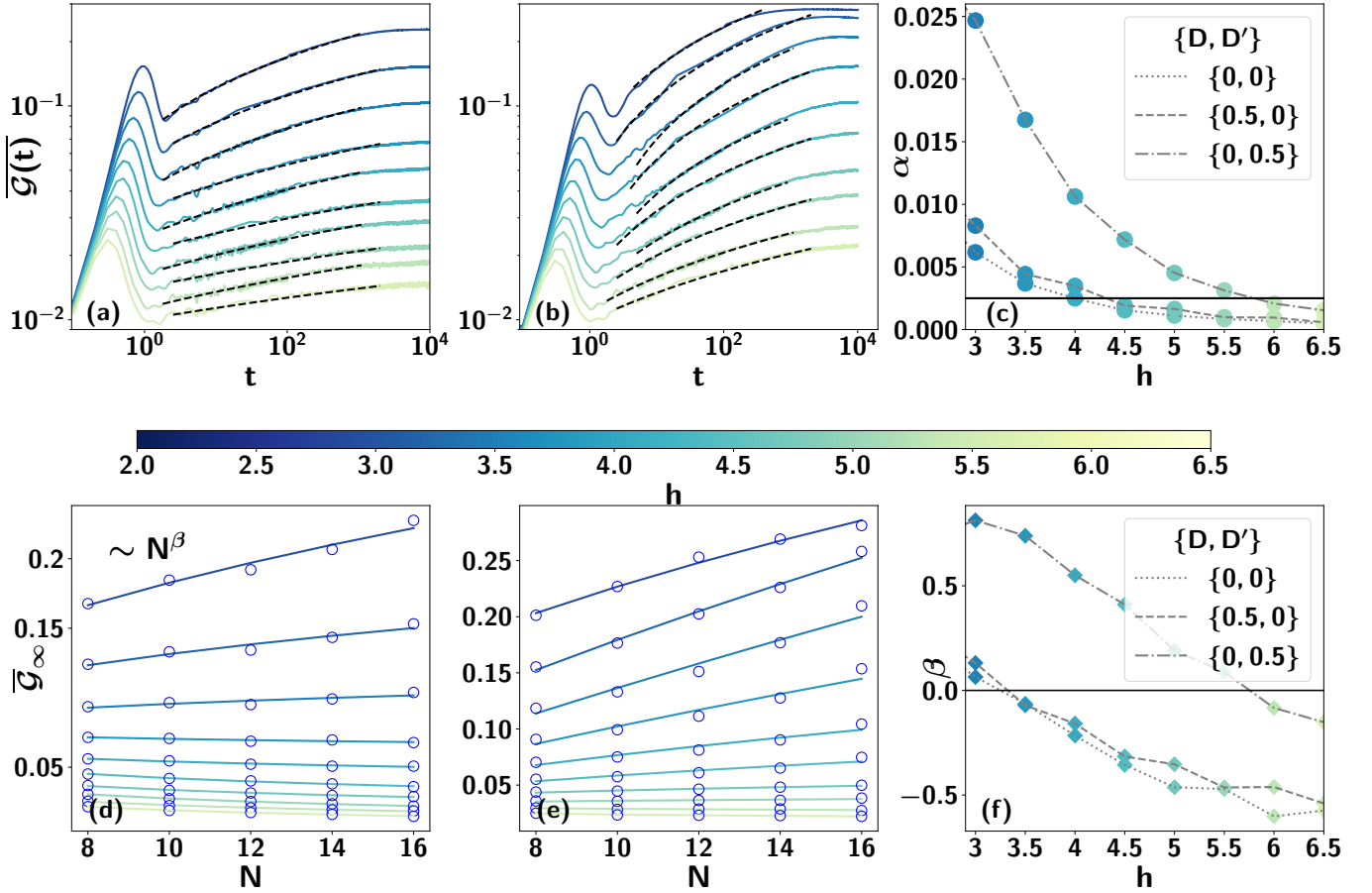


FIG. 7. Dynamics of genuine multipartite entanglement,  $\overline{\mathcal{G}}(t)$  (ordinate), and its scaling laws with respect to  $h$  (abscissa) for a disordered Heisenberg spin chain. Initializing in the Néel state,  $|\psi(0)\rangle = |0101 \dots 01\rangle$ , the system is evolved under the unitary operator  $e^{-iHt}$  corresponding to Eq. (1). *Transient regime* (upper panel) (a) The two-body DM is nonvanishing with  $D = 0.5$  and (b) both two- and three-body DM are non-zero with values as  $\{D, D'\} = \{0.5, 0.5\}$ . In both (a) and (b), each curve corresponds to a distinct disorder strength  $h$ , ranging from the ergodic regime ( $h = 1.0$ ) to deep many-body localized phases ( $h = 8.0$ ), as indicated in the legend. (c) The transient behavior of  $\overline{\mathcal{G}}(t)$  can be approximated by  $a \ln(t^\alpha) + b$ , where  $\alpha$  (ordinate) is the growth rate plotted with  $h$  (abscissa) for three different sets of values of  $\{D, D'\}$ . *Steady-state regime*. (Lower panel) (d) and (e)  $\overline{\mathcal{G}}_\infty$  (vertical axis) with  $N$  (horizontal axis) for two sets of  $D$  values as in (a) and (b). (f) Fitting  $\overline{\mathcal{G}}_\infty = cN^\beta + d$ , the exponent  $\beta$  (vertical axis) against  $h$  (horizontal axis) for three sets of  $D$  values as chosen in (c). Here,  $N = 16$ . All the axes are dimensionless.

is the logarithmic growth of the half-chain von Neumann entropy when a product state undergoes unitary dynamics governed by an MBL Hamiltonian [62]. This slow, yet steady, entanglement growth is widely recognized as a defining trait of interacting disordered systems, where strong correlations among numerous local degrees of freedom, such as spin orientations, are crucial. Notably, this behavior is absent in non-interacting settings, thereby serving as a key diagnostic of many-body effects.

At this point, it is important to emphasize that the half-block entropy captures entanglement solely across a single bipartition, thereby overlooking the genuinely multipartite character of quantum correlations that may emerge during the dynamics. To overcome this limitation and to gain a more complete understanding, we investigate the evolution of multipartite entanglement in terms of GGM in the MBL phase, following the methodology established in the preceding section.

We consider the Néel state,  $|\psi(0)\rangle = |0101 \dots 01\rangle$ , as the initial configuration and evolve it under a disordered interacting Hamiltonian, yielding the time-evolved state,  $|\psi(t)\rangle = e^{-iHt}|\psi(0)\rangle$ , where  $H$  is similar to the one mentioned in Eq. (1) but with open-boundary condition. Interestingly, the temporal behavior of GME averaged over multiple disorder realizations, indicated as  $\overline{\mathcal{G}}(t)$ , exhibits clear signatures that demarcate the MBL phase from the ergodic one, in agreement with conventional diagnostics such as the imbalance [62]. Note that  $\overline{\mathcal{G}}(t)$  only contains averaging over the disorder realization, unlike in the static case. The consistency of this observation across disorder realizations highlights the robustness of multipartite entanglement as an indicator of ergodicity breaking. To carry out this study for moderately large system sizes ( $N \sim 16$ ), we employ the Chebyshev polynomial expansion technique, which enables efficient simulation of real-time dynamics in disordered quantum systems (see Appendix



B).

At short times ( $t \lesssim 10$ ), all disorder strengths exhibit a rapid rise in GME due to the initial spreading of local wave packets, as seen in Figs. 7 (a) and (b). A characteristic peak around  $0 < t < 1$  is observed across all cases; this feature is attributed to the spreading of excitations up to the localization length and diminishes in magnitude with increasing  $h$  (cf. Ref. [61, 69, 120]). In the ergodic regime (e.g.  $h \leq 2$ ),  $\overline{\mathcal{G}}(t)$  reaches a high saturation value close to 0.3, indicating high multipartite entanglement typical of thermalizing systems. It is important to emphasize that while the bipartite von Neumann entropy may still exhibit logarithmic growth in the MBL regime due to interaction-induced dephasing, the genuine multipartite entanglement does not undergo a comparable rise. Instead, it remains largely bounded, suggesting that although local entanglement spreads, global multipartite entanglement remains constrained; a distinction that underscores the subtle nature of information dynamics in the localized phases. As  $h$  increases, both the peak height and the long-time saturation value of  $\overline{\mathcal{G}}(t)$  decrease, signaling the onset of localization. In the localized phase (e.g.,  $h \geq 4.0$ ), the growth is substantially suppressed and appears almost flat on the logarithmic time scale, except for minor transient behavior. In the preceding section, we observed that the presence of DM interactions shifts the localization transition to higher values of the disorder strength  $h$ , thereby extending the ergodic regime. We find that this trend persists in the dynamical study of multipartite entanglement as well. To quantitatively characterize the transition, we investigate the behavior of  $\overline{\mathcal{G}}(t)$  through two distinct regimes – (i) transient dynamics and (ii) steady-state saturation.

*Transient behavior.* The behavior of the dynamical entanglement in the period of  $2 \lesssim t \lesssim 1000$  can be effectively described by

$$\overline{\mathcal{G}}(t) = a \ln(t^\alpha) + b, \quad (10)$$

where  $a$  and  $\alpha$  capture the strength and the rate of entanglement growth, respectively, functions of disorder strength, and  $b$  is a constant. The growth rate  $\alpha$  decreases systematically with increasing  $h$ , indicating a gradual slowdown in the entanglement production as the system approaches the MBL regime, as shown in Fig. 7(c). Importantly, while the qualitative shape of  $\overline{\mathcal{G}}(t)$  remains similar across interaction settings  $\{D, D'\} = \{0, 0\}$  and  $\{0.5, 0\}$  (the plot of latter can be seen in Fig. 7 (a)), the critical disorder value at which  $\alpha$  effectively vanishes is shifted to higher  $h$  in the presence of nonvanishing two-body DM interaction. A more dramatic change is observed when three-body DM terms are present, i.e.,  $\{D, D'\} = \{0, 0.5\}$  in the Hamiltonian. This situation induces a significantly faster growth in  $\overline{\mathcal{G}}(t)$ , pushing the localization transition further into the strong-disorder regime (see Fig. 7(b)). To estimate the transition point quantitatively, we define  $\alpha = 0.0025$  as the numerical threshold below which the growth is effectively negligible. The resulting strengths of critical disorder are summarized in Table III, revealing a consistent delay in localization with added DM interaction. We note that the values reported here agree with the corresponding equilibrium results, thereby reinforcing the consistency of

| $D$ | $D'$ | $h^*$ |
|-----|------|-------|
| 0   | 0    | 4.0   |
| 0.5 | 0    | 4.6   |
| 0.0 | 0.5  | 5.9   |

TABLE III. Estimated critical disorder strength  $h^*$  for different DM interaction settings, obtained from the scaling behavior of GGM in the transient regime. In particular, the GGM in the period of  $2 \lesssim t \lesssim 1000$  follows a scaling law as  $\overline{\mathcal{G}}(t) = a \ln(t^\alpha) + b$ . The values of  $h^*$  are reported by setting  $\alpha = 0.0025$  as the transition threshold.

transient entanglement growth as a dynamical probe of localization.

*Steady-state scaling of GGM.* At sufficiently long times  $t \gtrsim 10^4$ , the multipartite entanglement, quantified via the disorder-averaged GGM, reaches a saturation value, represented as

$$\overline{\mathcal{G}}_\infty = \lim_{t \rightarrow \infty} \overline{\mathcal{G}}(t). \quad (11)$$

We observe that like in the equilibrium setting, this steady-state entanglement also serves as a sensitive probe for distinguishing between ergodic and many-body localized regimes. In the ergodic phase,  $\overline{\mathcal{G}}_\infty$  exhibits a growth with system-size  $N$ , suggestive of a sub-volume-law scaling and reflecting the delocalized nature of eigenstates. In contrast, the MBL phase is characterized by a near saturation and decline of  $\overline{\mathcal{G}}_\infty$  with increasing  $N$ , called as a sub-area-law behavior. These scaling features are encapsulated by the functional form as

$$\overline{\mathcal{G}}_\infty = cN^\beta + d, \quad (12)$$

where  $\beta$  defines the scaling exponent, and the coefficients  $c, d$  capture disorder-dependent offsets. We interpret the transition point as the critical disorder strength  $h^*$  at which  $\beta \rightarrow 0$ , signifying a loss of extensivity in multipartite entanglement, i.e., an archetypal signature of localization.

We study the variation of  $\overline{\mathcal{G}}_\infty$  with  $N$  for different disorder strengths and interaction parameters (see Figs. 7 (d) and (e)). The scaling behavior yields a monotonic decrease in  $\beta$  as disorder  $h$  increases. This dependence is summarized explicitly in Fig. 7 (f), where the extracted  $\beta$  values are plotted as a function of  $h$  for three different choices of Dzyaloshinskii-Moriya interaction strengths ( $D, D'$ ). Notably, the presence of either two-body ( $D \neq 0$ ) or three-body ( $D' \neq 0$ ) DM terms shifts the critical point  $h^*$  to larger values, implying an enhancement of ergodic behavior due to competing interaction-induced delocalization mechanisms.

In the ergodic phase, the value of  $\beta \in (0, 1)$  indicates a sub-volume law scaling that suggests the injected entanglement into the steady state survives for a longer duration. Interestingly, deeper into the localized phase, we observe the emergence of negative values of  $\beta$ , which we term to be sub-area-law ( $\beta < 0$ ), as shown in Fig. 7 (f), corresponding to a decreasing trend of  $\overline{\mathcal{G}}_\infty$  with  $N$ . This counterintuitive result signals that entanglement becomes increasingly suppressed

| $D$ | $D'$ | $h^*$ |
|-----|------|-------|
| 0   | 0    | 3.21  |
| 0.5 | 0    | 3.4   |
| 0.0 | 0.5  | 5.7   |

TABLE IV. Disorder strength  $h^*$  for transition estimated from steady-state entanglement ( $\bar{\mathcal{G}}_\infty$ ) scaling for various DM interaction configurations by setting the scaling parameter  $\beta \simeq 0$ .

with system size, a manifestation of the persistence of memory of the initial (product) state. Such negative scaling is most pronounced in the absence of the three-body DM interaction, indicating a more robust localization. We interpret this phenomenon as a strong signature of entanglement freezing in the deep MBL regime, where the breakdown of thermalization is so severe that even long-time dynamics fail to generate extensive correlations.

Recent experimental advances increasingly indicate that maintaining equilibrium across varying parameter regimes poses considerable challenges, particularly in strongly interacting quantum systems and the preparation of highly excited states [50]. In contrast, studying the system's out-of-equilibrium evolution, especially under nearly unitary conditions, has emerged as a more practical and insightful approach [39, 121] to probe the ergodic-to-MBL transition. Within this paradigm, our analysis demonstrates that the dynamics of genuine multipartite entanglement offer a powerful diagnostic of ergodicity-breaking. Specifically, the transient-time growth of entanglement follows a sub-logarithmic scaling,  $\bar{\mathcal{G}}(t) \sim \ln(t^\alpha)$ , while its long-time saturation value scales with system-size as  $\bar{\mathcal{G}}_\infty \sim N^\beta$ . Both the time exponent  $\alpha$  and the system-size exponent  $\beta$  exhibit sharp crossover behavior near the many-body localization transition, thereby serving as sensitive and robust indicators of the underlying phase structure. These findings reaffirm that multipartite entanglement dynamics captures the essential physics of the ergodic-to-MBL crossover, even in the absence of equilibrium assumptions.

## VI. CONCLUSION

Many-body localization (MBL) emerges from the interplay between disorder and interactions in quantum many-body systems, giving rise to emergent integrability. We explored here the transition from the ergodic to the MBL phase in disordered Heisenberg spin chains with additional two- and three-body Dzyaloshinskii–Moriya (DM) interactions under a disordered magnetic field. These asymmetric DM exchange interactions introduce new dynamics that significantly affect the localization properties of the system. To probe this transition, we employed the generalized geometric measure (GGM), a computable and reliable measure of genuine multipartite entanglement. While the measure generally involves optimizations over several bipartitions, we showed that in our considered model, it was sufficient to consider only the single-site

reduced states. This simplification made the GGM highly accessible, even for larger system sizes, and suitable for experimental implementation using current quantum simulators, both digital and analog alike. We mentioned that the resources required to measure GGM do not scale severely owing to the versatile randomized measurement toolbox.

Empowered with such an accessible measure, we examined the quenched average of GGM for states situated in the middle of the spectrum, within an equilibrium framework. We found that the corresponding scale-invariant disorder value robustly indicates the transition point from ergodic to localized phases. To validate this, we matched these values with standardized measures of long-range correlators and gap ratio. The results exhibit a strong agreement, reinforcing the effectiveness of multipartite entanglement as a marker of the transition. A notable and universal trend emerged from our study: in the presence of Dzyaloshinskii–Moriya interactions, the transition point shifts towards stronger disorder values, deep into the localized regime. We explained such a shift as a consequence of the injection of long-range correlation into the thermal eigenstates due to the DM interaction. Such correlations are typically seen in the presence of ergodic regimes, which require stronger disorder values to induce localization in the system.

We ventured into the non-equilibrium setting to study the dynamical behavior of the multipartite entanglement while starting with a product state that is energetically very close to the middle of the spectrum. In the transient regime, we found that the growth rate of GGM falls as the system transits into the localized phase. Notably, the disorder strength at which this transition occurs in the dynamical regime closely aligns with the critical point identified through equilibrium analysis. We further investigated the behavior of the steady-state entanglement as the system-size is varied. We found that a sub-area-law-like behavior is admitted when the system is in the localized phase, while in the ergodic phase, sub-volume-law scaling is observed, consistent with delocalized and thermalizing dynamics. These findings reinforce the utility of multipartite entanglement as a dynamical indicator of ergodic–MBL transitions.

## ACKNOWLEDGMENTS

We thank Sudipto Singha Roy for useful discussion. We acknowledge the use of the cluster computing facility at the Harish-Chandra Research Institute. This research was supported in part by the INFOSYS scholarship for senior students. T.S, K.D.A, and A.S.D acknowledge support from the project entitled "Technology Vertical - Quantum Communication" under the National Quantum Mission of the Department of Science and Technology (DST) (Sanction order No. Sanction Order No. DST/QTC/NQM/QComm/2024/2 (G)). LGCL is funded by the European Union. Views and opinions expressed are however those of the author(s) only and do not necessarily reflect those of the European Union or the European Commission. Neither the European Union nor the granting authority can be held responsible for them. This

project has received funding from the European Union's Horizon Europe research and innovation programme under grant agreement No 101080086 NeQST. This work was supported by the Provincia Autonoma di Trento, and Q@TN, the joint lab between University of Trento, FBK—Fondazione Bruno Kessler, INFN—National Institute for Nuclear Physics, and CNR—National Research Council, Italy.

## Appendix A: Numerical diagonalization

We use a recently developed polynomially filtered exact diagonalization (POLFED) [110], to obtain the eigenstates from the middle spectrum of the Hamiltonian (complex in our case) up to system-size  $N = 18$ . This approach is based on transforming the Hamiltonian via a polynomial function, such that the problem of finding the required spectrum of the original Hamiltonian is transformed into finding the extreme eigenspectrum (via the Lanczos method [122, 123]) of the transformed Hamiltonian. Specifically, for a finite normalized Hamiltonian (see Appendix B)  $\tilde{H} = \sum_{j=1}^M \varepsilon_j |\psi_j\rangle \langle \psi_j|$  with eigenvalues  $\varepsilon_j \in [-1, 1]$ , to find  $n_\varepsilon$  eigenvectors  $|\psi_j\rangle$  with eigenvalues close to  $\sigma$ , the function  $f_\sigma(\tilde{H})$  is used, such that the set  $\{\varepsilon_j\}$  close to  $\sigma$  are the extremal (minimum and/or maximum) eigenvalues of  $f_\sigma(\tilde{H})$ . Finally, to use the Lanczos algorithm, only  $f_\sigma(\tilde{H})|\Psi\rangle$  is needed to be computed for arbitrary  $|\Psi\rangle$ , without computing  $f_\sigma(\tilde{H})$  explicitly.

For example,  $f_\sigma(\tilde{H}) = (\tilde{H} - \sigma)^2$  can be used, which is a polynomial function of  $\tilde{H}$  which has high density of states near  $\sigma \sim 0$ , i.e., near the middle of the spectrum. Therefore in this case, the Lanczos algorithm faces convergence issues and is numerically unstable, as consecutive eigenvalues are very close to each other, and a gap is needed for numerical stability [122]. In the shift-invert approach,  $f_\sigma(\tilde{H}) = (\tilde{H} - \sigma I)^{-1}$ , is taken, where  $I$  is the identity matrix. Such a non-analytic function produces a numerically stable eigenspectrum of  $f_\sigma(\tilde{H})$  (only when  $\sigma \notin \{\varepsilon_j\}$ ) as  $\{\varepsilon_j\}$  close to  $\sigma$  have a gap inverse to the density of states near  $\sigma$ . The idea of POLFED is to expand the Dirac delta function  $\delta(x - \sigma)$  in terms of Chebyshev polynomials, i.e.,  $\delta(x - \sigma) = \sum_{p=0}^{\infty} c_p^\sigma T_p(x)$ , with  $c_p^\sigma = 2^{\min(1,p)} \cos(p \cos^{-1} \sigma)$  as the coefficients. This series is truncated to a finite order  $K$ , which is to be chosen based on the density of states of  $\tilde{H}$  near  $\sigma$  such that the  $n_\varepsilon$  eigenvectors have transformed eigenvalues in a single band. Therefore,

$$f_\sigma^K(\tilde{H}) = \frac{1}{D} \sum_{p=0}^K c_p^\sigma T_p(\tilde{H}), \quad (\text{A1})$$

is taken for a given  $K$ , and  $D$  is the normalization constant to ensure  $f_\sigma^K(\sigma) = 1$ , so that the maximum eigenvalue does not exceed 1. We use each  $\tilde{H}$  as a (complex) sparse matrix of Armadillo C++ library [109, 123] and the recursion relation of Chebyshev polynomials to compute  $f_\sigma^K(\tilde{H})|\Psi\rangle$  for arbitrary vector  $|\Psi\rangle$ . This multiplication is written as a function, which is fed to the Arnoldi method (as during the time of this

work, Armadillo does not support the complex sparse matrices for symmetric Lanczos method), by tweaking the 'eigs\_gen' function of Armadillo.

*Choice of  $K$ .* As shown in Ref. [110], for a given Hamiltonian  $\tilde{H}$ , the order  $K$  can be chosen before if the form of density of states of  $\tilde{H}$ . The guiding principle is that the lowest eigenvalue  $\theta_{\min}$  of  $f_\sigma^K(\tilde{H})$  satisfies  $\theta_{\min} > 0.17$ , as this is the value of a next maximum of  $f_\sigma^K(-1 \leq \varepsilon \leq 1)$ , the eigenvector corresponding to  $\theta_{\min}$  can be far away from  $\sigma$ . For a given  $n_\varepsilon$ ,  $\theta_{\min}$  keeps on decreasing, along with decreasing time required for diagonalization with increasing the value of  $K$ , as the  $f_\sigma^K(\tilde{H})$  becomes sharper near  $\sigma$  with increasing  $K$ . We keep  $K$  such that  $\theta_{\min} > 0.2$ , and obtain  $K = 60$  to  $100$  for  $N = 16$ , and  $K = 240$  to  $300$  for  $N = 18$  for different values of disorder strength  $h \in [0.5, 10.0]$  and DM interaction strengths  $D$  and  $D'$ .

Once the  $n_\varepsilon$  eigenvalues  $\{\theta_j\}$  and the corresponding eigenvectors  $\{|\psi_j\rangle\}$  are obtained with  $\min\{\theta_j\} > 0.2$ , the eigenvalues  $\{E_j\}$  of the original  $H$  are computed as  $E_j = \langle \psi_j | H | \psi_j \rangle$ , which are used to compute the level spacing ratios. The eigenvectors  $\{|\psi_j\rangle\}$  are used to compute the properties or observables of the system probed.

## Appendix B: Chebyshev polynomial expansion

The Chebyshev polynomial expansion provides a numerically stable and efficient method for simulating the time evolution of quantum states governed by a Hamiltonian [124, 125], specifically for large Hilbert space dimension. Given a quantum system described by a Hamiltonian  $H$  and an initial state  $|\psi(0)\rangle$ , the time-evolved state at time  $t$  is given by  $|\psi(t)\rangle = e^{-iHt}|\psi(0)\rangle$ . Instead of diagonalizing the Hamiltonian or using direct Taylor expansion, the Chebyshev method expands the evolution operator in terms of Chebyshev polynomials of the first kind,  $T_n(x)$ , which are defined over the interval  $[-1, 1]$ . To use this expansion, the Hamiltonian  $H$  must first be rescaled such that its spectrum lies within  $[-1, 1]$ . This is done via a linear transformation  $\tilde{H} = \frac{H-b}{a}$ , where  $a = \frac{E_{\max} - E_{\min}}{2}$  and  $b = \frac{E_{\max} + E_{\min}}{2}$ , with  $E_{\min}$  and  $E_{\max}$  being the minimum and maximum eigenvalues of  $H$ , respectively. The time evolution operator is then approximated by the series

$$e^{-iHt} \approx e^{-ibt} \sum_{n=0}^L a_n(t) T_n(\tilde{H}), \quad (\text{B1})$$

where the coefficients  $a_n(t) = 2^{\min(1,p)} (-i)^n J_n(at)$ ,  $J_n$  denotes the Bessel function of the first kind of order  $n$  and  $L \rightarrow \infty$  is the exact representation of the unitary. The application of Chebyshev polynomials to the state vector is performed recursively using the relations:  $|v_0\rangle = |\psi(0)\rangle$ ,  $|v_1\rangle = \tilde{H}|v_0\rangle$ , and  $|v_{n+1}\rangle = 2\tilde{H}|v_n\rangle - |v_{n-1}\rangle$ . The final evolved state is then computed as  $|\psi(t)\rangle = e^{-ibt} \sum_{n=0}^L a_n(t) |v_n\rangle$ . The series is truncated at finite  $L \approx \max(30, 2at)$  (Appendix C of [31]), with at least 30 terms for convergence checked with  $|a_n(t)| |v_L\rangle| < \epsilon_m (= 10^{-10})$ , where  $\epsilon_m$  is the error of approximation, and can be set either by machine-precision, or

precision of Lanczos method while normalizing the Hamiltonian. This method is especially advantageous for large sparse

Hamiltonian, as it is stable and only requires successive applications of the Hamiltonian (or its rescaled form) to vectors, without the need for full diagonalization.

- 
- [1] J. M. Deutsch, Quantum statistical mechanics in a closed system, *Phys. Rev. A* **43**, 2046 (1991).
  - [2] M. Srednicki, Chaos and quantum thermalization, *Phys. Rev. E* **50**, 888 (1994).
  - [3] J. M. Deutsch, Eigenstate thermalization hypothesis, *Reports on Progress in Physics* **81**, 082001 (2018).
  - [4] L. D'Alessio, Y. Kafri, A. Polkovnikov, and M. Rigol, From quantum chaos and eigenstate thermalization to statistical mechanics and thermodynamics, *Advances in Physics* **65**, 239 (2016), <https://doi.org/10.1080/00018732.2016.1198134>.
  - [5] M. L. Mehta, *Random Matrices* (Elsevier, 1991).
  - [6] F. Haake, *Quantum Signatures of Chaos* (Springer Berlin Heidelberg, 2010).
  - [7] Y. Y. Atas, E. Bogomolny, O. Giraud, and G. Roux, Distribution of the ratio of consecutive level spacings in random matrix ensembles, *Phys. Rev. Lett.* **110**, 084101 (2013).
  - [8] E. P. Wigner, On the statistical distribution of the widths and spacings of nuclear resonance levels, *Mathematical Proceedings of the Cambridge Philosophical Society* **47**, 790–798 (1951).
  - [9] F. J. Dyson, The threefold way. algebraic structure of symmetry groups and ensembles in quantum mechanics, *Journal of Mathematical Physics* **3**, 1199 (1962), [https://pubs.aip.org/aip/jmp/article-pdf/3/6/1199/19064331/1199\\_1\\_online.pdf](https://pubs.aip.org/aip/jmp/article-pdf/3/6/1199/19064331/1199_1_online.pdf).
  - [10] M. Rigol, V. Dunjko, and M. Olshanii, Thermalization and its mechanism for generic isolated quantum systems, *Nature* **452**, 854–858 (2008).
  - [11] C. J. Turner, A. A. Michailidis, D. A. Abanin, M. Serbyn, and Z. Papić, Weak ergodicity breaking from quantum many-body scars, *Nature Physics* **14**, 745 (2018).
  - [12] A. Chandran, T. Iadecola, V. Khemani, and R. Moessner, Quantum many-body scars: A quasiparticle perspective, *Annual Review of Condensed Matter Physics* **14**, 443 (2023).
  - [13] M. Schulz, C. A. Hooley, R. Moessner, and F. Pollmann, Stark many-body localization, *Phys. Rev. Lett.* **122**, 040606 (2019).
  - [14] P. Ponte, Z. Papić, F. m. c. Huveneers, and D. A. Abanin, Many-body localization in periodically driven systems, *Phys. Rev. Lett.* **114**, 140401 (2015).
  - [15] D. V. Else, B. Bauer, and C. Nayak, Floquet time crystals, *Phys. Rev. Lett.* **117**, 090402 (2016).
  - [16] G. Cipolloni and J. Kudler-Flam, Non-hermitian hamiltonians violate the eigenstate thermalization hypothesis, *Phys. Rev. B* **109**, L020201 (2024).
  - [17] F. Roccati, F. Balducci, R. Shir, and A. Chenu, Diagnosing non-hermitian many-body localization and quantum chaos via singular value decomposition, *Phys. Rev. B* **109**, L140201 (2024).
  - [18] P. W. Anderson, Absence of diffusion in certain random lattices, *Phys. Rev.* **109**, 1492 (1958).
  - [19] V. Oganesyan and D. A. Huse, Localization of interacting fermions at high temperature, *Phys. Rev. B* **75**, 155111 (2007).
  - [20] A. Pal and D. A. Huse, Many-body localization phase transition, *Phys. Rev. B* **82**, 174411 (2010).
  - [21] S. Bera, G. De Tomasi, F. Weiner, and F. Evers, Density propagator for many-body localization: Finite-size effects, transient subdiffusion, and exponential decay, *Phys. Rev. Lett.* **118**, 196801 (2017).
  - [22] J. A. Kjäll, J. H. Bardarson, and F. Pollmann, Many-body localization in a disordered quantum ising chain, *Phys. Rev. Lett.* **113**, 107204 (2014).
  - [23] R. Mondaini and M. Rigol, Many-body localization and thermalization in disordered hubbard chains, *Phys. Rev. A* **92**, 041601 (2015).
  - [24] P. Sierant, D. Delande, and J. Zakrzewski, Many-body localization due to random interactions, *Phys. Rev. A* **95**, 021601 (2017).
  - [25] P. Sierant and J. Zakrzewski, Many-body localization of bosons in optical lattices, *New Journal of Physics* **20**, 043032 (2018).
  - [26] N. Y. Yao, C. R. Laumann, S. Gopalakrishnan, M. Knap, M. Müller, E. A. Demler, and M. D. Lukin, Many-body localization in dipolar systems, *Phys. Rev. Lett.* **113**, 243002 (2014).
  - [27] A. L. Burin, Many-body delocalization in a strongly disordered system with long-range interactions: Finite-size scaling, *Phys. Rev. B* **91**, 094202 (2015).
  - [28] H. Li, J. Wang, X.-J. Liu, and H. Hu, Many-body localization in ising models with random long-range interactions, *Phys. Rev. A* **94**, 063625 (2016).
  - [29] R. M. Nandkishore and S. L. Sondhi, Many-body localization with long-range interactions, *Phys. Rev. X* **7**, 041021 (2017).
  - [30] K. S. Tikhonov and A. D. Mirlin, Many-body localization transition with power-law interactions: Statistics of eigenstates, *Phys. Rev. B* **97**, 214205 (2018).
  - [31] P. Sierant, K. Biedroń, G. Morigi, and J. Zakrzewski, Many-body localization in presence of cavity mediated long-range interactions, *SciPost Physics* **7**, 10.21468/scipostphys.7.1.008 (2019).
  - [32] V. Khemani, D. N. Sheng, and D. A. Huse, Two universality classes for the many-body localization transition, *Phys. Rev. Lett.* **119**, 075702 (2017).
  - [33] S.-X. Zhang and H. Yao, Universal properties of many-body localization transitions in quasiperiodic systems, *Phys. Rev. Lett.* **121**, 206601 (2018).
  - [34] M. Serbyn, Z. Papić, and D. A. Abanin, Local conservation laws and the structure of the many-body localized states, *Phys. Rev. Lett.* **111**, 127201 (2013).
  - [35] D. A. Huse, R. Nandkishore, and V. Oganesyan, Phenomenology of fully many-body-localized systems, *Phys. Rev. B* **90**, 174202 (2014).
  - [36] J. Z. Imbrie, On many-body localization for quantum spin chains, *Journal of Statistical Physics* **163**, 998 (2016).
  - [37] J. Smith, A. Lee, P. Richerme, B. Neyenhuis, P. W. Hess, P. Hauke, M. Heyl, D. A. Huse, and C. Monroe, Many-body localization in a quantum simulator with programmable random disorder, *Nature Physics* **12**, 907 (2016).
  - [38] S. S. Kondov, W. R. McGehee, W. Xu, and B. DeMarco, Disorder-induced localization in a strongly correlated atomic hubbard gas, *Phys. Rev. Lett.* **114**, 083002 (2015).
  - [39] M. Schreiber, S. S. Hodgman, P. Bordia, H. P. Lüschen, M. H. Fischer, R. Vosk, E. Altman, U. Schneider, and I. Bloch, Ob-



- servation of many-body localization of interacting fermions in a quasirandom optical lattice, *Science* **349**, 842 (2015).
- [40] J.-y. Choi, S. Hild, J. Zeiher, P. Schauß, A. Rubio-Abadal, T. Yefsah, V. Khemani, D. A. Huse, I. Bloch, and C. Gross, Exploring the many-body localization transition in two dimensions, *Science* **352**, 1547 (2016).
- [41] M. Rispoli, A. Lukin, R. Schittko, S. Kim, M. E. Tai, J. Léonard, and M. Greiner, Quantum critical behaviour at the many-body localization transition, *Nature* **573**, 385 (2019).
- [42] T. Kohlert, S. Scherg, X. Li, H. P. Lüschen, S. Das Sarma, I. Bloch, and M. Aidelsburger, Observation of many-body localization in a one-dimensional system with a single-particle mobility edge, *Phys. Rev. Lett.* **122**, 170403 (2019).
- [43] Q. Guo, C. Cheng, Z.-H. Sun, Z. Song, H. Li, Z. Wang, W. Ren, H. Dong, D. Zheng, Y.-R. Zhang, R. Mondaini, H. Fan, and H. Wang, Observation of energy-resolved many-body localization, *Nature Physics* **17**, 234 (2020).
- [44] M. Gong, G. D. de Moraes Neto, C. Zha, Y. Wu, H. Rong, Y. Ye, S. Li, Q. Zhu, S. Wang, Y. Zhao, F. Liang, J. Lin, Y. Xu, C.-Z. Peng, H. Deng, A. Bayat, X. Zhu, and J.-W. Pan, Experimental characterization of the quantum many-body localization transition, *Phys. Rev. Res.* **3**, 033043 (2021).
- [45] F. Alet and N. Laflorencie, Many-body localization: An introduction and selected topics, *Comptes Rendus Physique* **19**, 498 (2018), quantum simulation / Simulation quantique.
- [46] R. Nandkishore and D. A. Huse, Many-body localization and thermalization in quantum statistical mechanics, *Annual Review of Condensed Matter Physics* **6**, 15–38 (2015).
- [47] W. De Roeck and F. m. c. Huveneers, Stability and instability towards delocalization in many-body localization systems, *Phys. Rev. B* **95**, 155129 (2017).
- [48] D. A. Abanin, E. Altman, I. Bloch, and M. Serbyn, Colloquium: Many-body localization, thermalization, and entanglement, *Rev. Mod. Phys.* **91**, 021001 (2019).
- [49] P. Sierant and J. Zakrzewski, Challenges to observation of many-body localization, *Phys. Rev. B* **105**, 224203 (2022).
- [50] P. Sierant, M. Lewenstein, A. Scardicchio, L. Vidmar, and J. Zakrzewski, Many-body localization in the age of classical computing, *Reports on Progress in Physics* **88**, 026502 (2025).
- [51] M. Serbyn and J. E. Moore, Spectral statistics across the many-body localization transition, *Phys. Rev. B* **93**, 041424 (2016).
- [52] L. Colmenarez, P. A. McClarty, M. Haque, and D. J. Luitz, Statistics of correlation functions in the random Heisenberg chain, *SciPost Phys.* **7**, 064 (2019).
- [53] J. Colbois, F. Alet, and N. Laflorencie, Statistics of systemwide correlations in the random-field xxz chain: Importance of rare events in the many-body localized phase, *Phys. Rev. B* **110**, 214210 (2024).
- [54] B. Bauer and C. Nayak, Area laws in a many-body localized state and its implications for topological order, *Journal of Statistical Mechanics: Theory and Experiment* **2013**, P09005 (2013).
- [55] D. A. Huse, R. Nandkishore, V. Oganesyan, A. Pal, and S. L. Sondhi, Localization-protected quantum order, *Phys. Rev. B* **88**, 014206 (2013).
- [56] A. Chandran, V. Khemani, C. R. Laumann, and S. L. Sondhi, Many-body localization and symmetry-protected topological order, *Phys. Rev. B* **89**, 144201 (2014).
- [57] Y. Bahri, R. Vosk, E. Altman, and A. Vishwanath, Localization and topology protected quantum coherence at the edge of hot matter, *Nature Communications* **6**, 10.1038/ncomms8341 (2015).
- [58] A. Prakash, S. Ganeshan, L. Fidkowski, and T.-C. Wei, Eigenstate phases with finite on-site non-abelian symmetry, *Phys. Rev. B* **96**, 165136 (2017).
- [59] A. J. Friedman, R. Vasseur, A. C. Potter, and S. A. Parameswaran, Localization-protected order in spin chains with non-abelian discrete symmetries, *Phys. Rev. B* **98**, 064203 (2018).
- [60] K. Agarwal, S. Gopalakrishnan, M. Knap, M. Müller, and E. Demler, Anomalous diffusion and griffiths effects near the many-body localization transition, *Phys. Rev. Lett.* **114**, 160401 (2015).
- [61] J.-J. Chen, K. Xu, L.-H. Ren, Y.-R. Zhang, and H. Fan, Dynamics of quantum coherence in many-body localized systems, *Phys. Rev. A* **110**, 022434 (2024).
- [62] D. J. Luitz, N. Laflorencie, and F. Alet, Extended slow dynamical regime close to the many-body localization transition, *Phys. Rev. B* **93**, 060201 (2016).
- [63] E. V. H. Doggen, F. Schindler, K. S. Tikhonov, A. D. Mirlin, T. Neupert, D. G. Polyakov, and I. V. Gornyi, Many-body localization and delocalization in large quantum chains, *Phys. Rev. B* **98**, 174202 (2018).
- [64] T. Chanda and J. Zakrzewski, Many-body localization regime for cavity-induced long-range interacting models, *Phys. Rev. B* **105**, 054309 (2022).
- [65] F. Formicola, G. Di Bello, G. De Filippis, V. Cataudella, D. Farina, and C. A. Perroni, *Local ergotropy dynamically witnesses many-body localized phases* (2025).
- [66] J. H. Bardarson, F. Pollmann, and J. E. Moore, Unbounded growth of entanglement in models of many-body localization, *Phys. Rev. Lett.* **109**, 017202 (2012).
- [67] M. Serbyn, Z. Papić, and D. A. Abanin, Universal slow growth of entanglement in interacting strongly disordered systems, *Phys. Rev. Lett.* **110**, 260601 (2013).
- [68] S. D. Geraedts, N. Regnault, and R. M. Nandkishore, Characterizing the many-body localization transition using the entanglement spectrum, *New Journal of Physics* **19**, 113021 (2017).
- [69] P. R. N. Falcão, P. Sierant, J. Zakrzewski, and E. Tirrito, *Magic dynamics in many-body localized systems* (2025), arXiv:2503.07468 [quant-ph].
- [70] R. Singh, J. H. Bardarson, and F. Pollmann, Signatures of the many-body localization transition in the dynamics of entanglement and bipartite fluctuations, *New Journal of Physics* **18**, 023046 (2016).
- [71] Ángel L. Corps, R. A. Molina, , and A. Relaño, Signatures of a critical point in the many-body localization transition, *SciPost Phys.* **10**, 107 (2021).
- [72] D. J. Luitz, N. Laflorencie, and F. Alet, Many-body localization edge in the random-field heisenberg chain, *Phys. Rev. B* **91**, 081103 (2015).
- [73] F. Anza, F. Pietracaprina, and J. Goold, Logarithmic growth of local entropy and total correlations in many-body localized dynamics, *Quantum* **4**, 250 (2020).
- [74] A. S. Aramthottil, T. Chanda, P. Sierant, and J. Zakrzewski, Finite-size scaling analysis of the many-body localization transition in quasiperiodic spin chains, *Phys. Rev. B* **104**, 214201 (2021).
- [75] F. Iemini, A. Russomanno, D. Rossini, A. Scardicchio, and R. Fazio, Signatures of many-body localization in the dynamics of two-site entanglement, *Phys. Rev. B* **94**, 214206 (2016).
- [76] S. Bera and A. Lakshminarayan, Local entanglement structure across a many-body localization transition, *Phys. Rev. B* **93**, 134204 (2016).
- [77] G. De Tomasi, Algebraic many-body localization and its implications on information propagation, *Phys. Rev. B* **99**, 054204 (2019).

- [78] A. Safavi-Naini, M. L. Wall, O. L. Acevedo, A. M. Rey, and R. M. Nandkishore, Quantum dynamics of disordered spin chains with power-law interactions, *Phys. Rev. A* **99**, 033610 (2019).
- [79] A. S. Sajna and A. Polkovnikov, Semiclassical dynamics of a disordered two-dimensional hubbard model with long-range interactions, *Phys. Rev. A* **102**, 033338 (2020).
- [80] F. Perciavalle, *Multipartite entanglement in many-body localized quantum systems*, Master's thesis, University of Pisa (2021).
- [81] Z.-C. Yang, C. Chamon, A. Hamma, and E. R. Mucciolo, Two-component structure in the entanglement spectrum of highly excited states, *Phys. Rev. Lett.* **115**, 267206 (2015).
- [82] M. Serbyn, A. A. Michailidis, D. A. Abanin, and Z. Papić, Power-law entanglement spectrum in many-body localized phases, *Phys. Rev. Lett.* **117**, 160601 (2016).
- [83] J. Gray, S. Bose, and A. Bayat, Many-body localization transition: Schmidt gap, entanglement length, and scaling, *Phys. Rev. B* **97**, 201105 (2018).
- [84] G. De Tomasi, S. Bera, J. H. Bardarson, and F. Pollmann, Quantum mutual information as a probe for many-body localization, *Phys. Rev. Lett.* **118**, 016804 (2017).
- [85] J. Gray, A. Bayat, A. Pal, and S. Bose, Scale invariant entanglement negativity at the many-body localization transition, *arXiv:1908.02761* (2019).
- [86] C. H. Bennett, S. Popescu, D. Rohrlich, J. A. Smolin, and A. V. Thapliyal, Exact and asymptotic measures of multipartite pure-state entanglement, *Phys. Rev. A* **63**, 012307 (2000).
- [87] J. Eisert and H. J. Briegel, Schmidt measure as a tool for quantifying multiparticle entanglement, *Phys. Rev. A* **64**, 022306 (2001).
- [88] F. Verstraete, J. Dehaene, and B. De Moor, Normal forms and entanglement measures for multipartite quantum states, *Phys. Rev. A* **68**, 012103 (2003).
- [89] T.-C. Wei and P. M. Goldbart, Geometric measure of entanglement and applications to bipartite and multipartite quantum states, *Phys. Rev. A* **68**, 042307 (2003).
- [90] Z.-H. Ma, Z.-H. Chen, J.-L. Chen, C. Spengler, A. Gabriel, and M. Huber, Measure of genuine multipartite entanglement with computable lower bounds, *Phys. Rev. A* **83**, 062325 (2011).
- [91] S. M. Hashemi Rafsanjani, M. Huber, C. J. Broadbent, and J. H. Eberly, Genuinely multipartite concurrence of  $n$ -qubit  $x$  matrices, *Phys. Rev. A* **86**, 062303 (2012).
- [92] A. Sen(De) and U. Sen, Channel capacities versus entanglement measures in multiparty quantum states, *Phys. Rev. A* **81**, 012308 (2010).
- [93] I. Dzyaloshinsky, A thermodynamic theory of "weak" ferromagnetism of antiferromagnetics, *Journal of Physics and Chemistry of Solids* **4**, 241 (1958).
- [94] T. Moriya, Anisotropic superexchange interaction and weak ferromagnetism, *Phys. Rev.* **120**, 91 (1960).
- [95] T. Moriya, New mechanism of anisotropic superexchange interaction, *Phys. Rev. Lett.* **4**, 228 (1960).
- [96] R. Jafari, M. Kargarian, A. Langari, and M. Siahatgar, Phase diagram and entanglement of the ising model with dzyaloshinskii-moriya interaction, *Phys. Rev. B* **78**, 214414 (2008).
- [97] Q. Luo, Analytical results for the unusual grüneisen ratio in the quantum ising model with dzyaloshinskii-moriya interaction, *Phys. Rev. B* **105**, L060401 (2022).
- [98] T. K. Konar, L. G. C. Lakkaraju, and A. Sen(De), Slow decay rate of correlations induced by long-range extended dzyaloshinskii-moriya interactions, *Phys. Rev. A* **111**, 052402 (2025).
- [99] M. Kargarian, R. Jafari, and A. Langari, Dzyaloshinskii-moriya interaction and anisotropy effects on the entanglement of the heisenberg model, *Phys. Rev. A* **79**, 042319 (2009).
- [100] S. Roy, T. Chanda, T. Das, D. Sadhukhan, A. Sen(De), and U. Sen, Phase boundaries in an alternating-field quantum xy model with dzyaloshinskii-moriya interaction: Sustainable entanglement in dynamics, *Phys. Rev. B* **99**, 064422 (2019).
- [101] Z. Ming, X. Hui, L. Xiao-Xian, and T. Pei-Qing, The effects of the Dzyaloshinskii—Moriya interaction on the ground-state properties of the XY chain in a transverse field, *Chin. Phys. B* **22**, 090313 (2013).
- [102] Z.-A. Liu, T.-C. Yi, J.-H. Sun, Y.-L. Dong, and W.-L. You, Lifshitz phase transitions in a one-dimensional gamma model, *Phys. Rev. E* **102**, 032127 (2020).
- [103] D. C. Dender, D. Davidović, D. H. Reich, C. Broholm, K. Lefmann, and G. Aeppli, Magnetic properties of a quasi-one-dimensional  $s=1/2$  antiferromagnet: Copper benzoate, *Phys. Rev. B* **53**, 2583 (1996).
- [104] D. C. Dender, P. R. Hammar, D. H. Reich, C. Broholm, and G. Aeppli, Direct observation of field-induced incommensurate fluctuations in a one-dimensional  $S = 1/2$  antiferromagnet, *Phys. Rev. Lett.* **79**, 1750 (1997).
- [105] M. Kohgi, K. Iwasa, J.-M. Mignot, B. Fåk, P. Gegenwart, M. Lang, A. Ochiai, H. Aoki, and T. Suzuki, Staggered field effect on the one-dimensional  $S = \frac{1}{2}$  antiferromagnet  $\text{Yb}_4\text{As}_3$ , *Phys. Rev. Lett.* **86**, 2439 (2001).
- [106] P. Fulde, B. Schmidt, and P. Thalmeier, Theoretical model for the semi-metal  $\text{Yb}_4\text{As}_3$ , *Europhysics Letters* **31**, 323 (1995).
- [107] S. Stagraczynski, P. Balaz, M. Jafari, J. Barnas, and A. Dyrdal, Magnetic ordering and dynamics in monolayers and bilayers of chromium trihalides: atomistic simulations approach (2024), *arXiv:2404.15543 [cond-mat.mes-hall]*.
- [108] S. Stagraczyński, L. Chotorlishvili, M. Schüller, M. Mierzejewski, and J. Berakdar, Many-body localization phase in a spin-driven chiral multiferroic chain, *Phys. Rev. B* **96**, 054440 (2017).
- [109] C. Sanderson and R. Curtin, Armadillo: an efficient framework for numerical linear algebra, in *2025 17th International Conference on Computer and Automation Engineering (IC-CAE)* (2025) pp. 303–307.
- [110] P. Sierant, M. Lewenstein, and J. Zakrzewski, Polynomially filtered exact diagonalization approach to many-body localization, *Phys. Rev. Lett.* **125**, 156601 (2020).
- [111] A. SHIMONY, Degree of entanglement, *Annals of the New York Academy of Sciences* **755**, 675 (1995), <https://nyaspubs.onlinelibrary.wiley.com/doi/pdf/10.1111/j.1749-6632.1995.tb39008.x>.
- [112] H. Barnum and N. Linden, Monotones and invariants for multi-particle quantum states, *Journal of Physics A: Mathematical and General* **34**, 6787 (2001).
- [113] A. Elben, S. T. Flammia, H.-Y. Huang, R. Kueng, J. Preskill, B. Vermersch, and P. Zoller, The randomized measurement toolbox, *Nature Reviews Physics* **5**, 9 (2023).
- [114] H. Weyl, Das asymptotische Verteilungsgesetz der Eigenwerte linearer partieller Differentialgleichungen (mit einer Anwendung auf die Theorie der Hohlraumstrahlung), *Math. Ann.* **71**, 441 (1912).
- [115] D. Gross, S. T. Flammia, and J. Eisert, Most quantum states are too entangled to be useful as computational resources, *Phys. Rev. Lett.* **102**, 190501 (2009).
- [116] M. J. Bremner, C. Mora, and A. Winter, Are random pure states useful for quantum computation?, *Phys. Rev. Lett.* **102**, 190502 (2009).

- [117] S. Rethinasamy, S. Roy, T. Chanda, A. Sen(De), and U. Sen, Universality in distribution of monogamy scores for random multiqubit pure states, [Phys. Rev. A \*\*99\*\*, 042302 \(2019\)](#).
- [118] M. Kunimi, T. Tomita, H. Katsura, and Y. Kato, Proposal for simulating quantum spin models with the dzyaloshinskii-moriya interaction using rydberg atoms and the construction of asymptotic quantum many-body scar states, [Phys. Rev. A \*\*110\*\*, 043312 \(2024\)](#).
- [119] J. Šuntajs, J. Bonča, T. c. v. Prosen, and L. Vidmar, Ergodicity breaking transition in finite disordered spin chains, [Phys. Rev. B \*\*102\*\*, 064207 \(2020\)](#).
- [120] F. Formicola, G. D. Bello, G. D. Filippis, V. Cataudella, D. Farina, and C. A. Perroni, [Local ergotropy dynamically witnesses many-body localized phases](#) (2025), [arXiv:2502.20002 \[quant-ph\]](#).
- [121] H. P. Lüschen, P. Bordia, S. Scherg, F. Alet, E. Altman, U. Schneider, and I. Bloch, Observation of slow dynamics near the many-body localization transition in one-dimensional quasiperiodic systems, [Phys. Rev. Lett. \*\*119\*\*, 260401 \(2017\)](#).
- [122] C. Lanczos, An iteration method for the solution of the eigenvalue problem of linear differential and integral operators, [Journal of Research of the National Bureau of Standards \*\*45\*\*, 255 \(1950\)](#).
- [123] C. Sanderson and R. Curtin, Practical sparse matrices in c++ with hybrid storage and template-based expression optimisation, [Mathematical and Computational Applications \*\*24\*\*, 10.3390/mca24030070 \(2019\)](#).
- [124] A. Weiße, G. Wellein, A. Alvermann, and H. Fehske, The kernel polynomial method, [Rev. Mod. Phys. \*\*78\*\*, 275 \(2006\)](#).
- [125] A. Weiße and H. Fehske, Chebyshev expansion techniques, in [Computational Many-Particle Physics](#), edited by H. Fehske, R. Schneider, and A. Weiße (Springer Berlin Heidelberg, Berlin, Heidelberg, 2008) pp. 545–577.